JOURNAL OF APPLIED ELECTROCHEMISTRY 25 (1995) 1031–1037

Anodic behaviour of zirconium and its alloys in fluorinated nitric media Dissolution-passivation model

J. PRONO, T. JASZAY

Ecole Centrale de Nantes, 1 rue de la Noë, 44072 Nantes, Cedex 03, France

A. CAPRANI

LBHP, Univ. Paris VII, 2 place Jussieu, 75251 Paris, Cedex 05, France

J. P. FRAYRET

LMP, Univ. Bordeaux I, 351 Cours de la Libération, 33405 Talence, Cedex, France

Received 3 December 1993; revised 7 April 1995

Current–potential curves for zirconium in fluorinated nitric medium were obtained using a rotating disc electrode. The curves exhibited four different domains according to the potential, and suggested a seven-step reaction model composed of three competing paths. Quantitatively verified by comparing computed and experimental curves, this model accounts for the behaviour of either zirconium or its main industrial alloy, Zircaloy 4, over potentials ranging from the corrosion potential up to the zirconia passivation potential. Moreover, the model allows the rate of elementary steps to be determined, as well as the coverage ratio of the intermediate species considered. These results correlated with scanning electron microscopy observations and proved to be particularly sensitive to slight modifications of the electrochemical system. The model can also be considered as a promising tool in the study of zirconium alloy pickling in acidic media and for optimising the resulting surface quality.

1. Introduction

In a previous study [1], we investigated the behaviour of a rotating disc electrode (RDE) of zirconium in fluorinated nitric medium from the corrosion potential (approx. −800 mV vs SCE) up to +1000 mV vs SCE. Three intermediate adsorbed species, noted Zr^{III}_{ads}, Zr^{IV}_{ads1} and Zr^{IV}_{ads2}, were considered as a minimum to explain the shape of the current–potential curve presented in Fig. 1. Assuming that the adsorbed species satisfy the conditions of Langmuir's isotherm [2, 3], we constructed a reaction model (Fig. 2) composed of five steps and one bifurcation to account for the shape of the I/E curve. The model was validated by the good correlation between experimental current values and the computed curve, using an optimization method presented elsewhere [4–6]. A computer program [7] based on the simplex method was also used to determine the kinetic rates of each step.

This model was intentionally limited to potentials lower than +1000 mV vs SCE because the stability and reproducibility of experimental measurements necessary for this kind of study were not sufficient at higher potentials. Although such instability is frequently encountered with electrochemical systems depending on mass transport [8, 9], it can generally be prevented by using a rotating disc electrode if the experimental conditions correspond to the particular requirements of the system studied [10, 11].

Here, we further investigated the behaviour of zirconium in fluorinated nitric media by using potentials higher than +1000 mV vs SCE and an improved experimental procedure.

2. Experimental procedure

Measurements were made with zirconium (Van Arkel) and Zircaloy 4 (Cezus, France), whose compositions are given in Table 1. The rotating disc electrode was the cross-section of a cylinder 5 mm in diameter, its cylindrical surface being covered by a thermo-shrinkable insulating sheath. The disc was polished using SiC abrasive paper up to grade 500. The electrode rotation speed was 500 rpm. Particular care was taken when preparing the rotating system to ensure maximum stability: polishing was carried out on a plateau with a specific guidance device to obtain very good perpendicularity, and the maximum eccentricity of the disc was less than 0.1 mm.

A PTFE cell maintained at 25° C was filled with a mixture of sodium fluoride (0.12 mol dm^{-3}) and nitric acid (7.0 mol dm^{-3}) deaerated by argon U-bubbling (the device was located above the disc in order to limit hydrodynamic disturbances of the active surface). This medium was chosen to simulate the

0021-891X

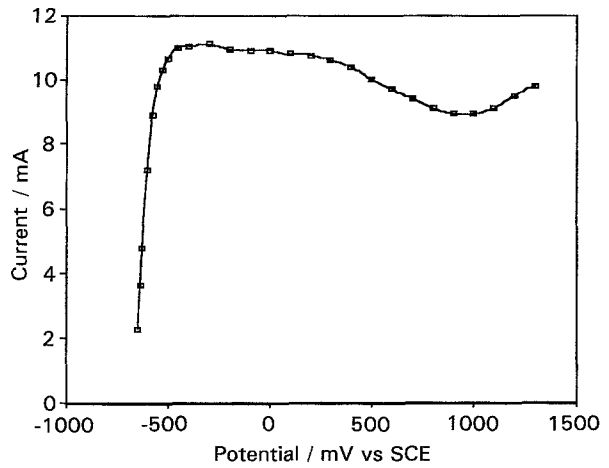

Fig. 1. Current–potential curve for Zircaloy 4 in (NaF: 0.12 M + HNO_3: 7 M); diam. 5 mm; 500 rpm; 25 °C.

industrial pickling bath composition used for the preparation of nuclear fuel cladding tubes. It gives a moderated dissolution rate, meaning that the influence of medium composition variations during the experiment can be neglected.

The counter electrode was a large platinum grid and the reference electrode was an Ag/AgCl electrode saturated with KCl (all results are presented with respect to the saturated calomel electrode potential SCE). Measurements were performed using a potentiostat. Steady-state current–potential curves were recorded from the corrosion potential in the anodic direction. A steady-state current was generally obtained after 15 min. However, with potentials higher than +1000 mV vs SCE, the stabilization time increased to several hours.

The valence state of dissolved ions must be known to formulate a reaction model. Valence state was calculated at constant potential from the electrode mass loss and by directly applying Faraday's law; polarization time was 2 h.

Samples for examination by SEM were polarized for 1 h at different potentials from polished surfaces (grade 500 SiC).

3. Results

3.1. *Steady-state current–potential curves*

These rigorous experimental conditions considerably improved the stability and reproducibility of measurements. The current–potential profiles presented in Fig. 3 for zirconium and Zircaloy 4 are very similar,

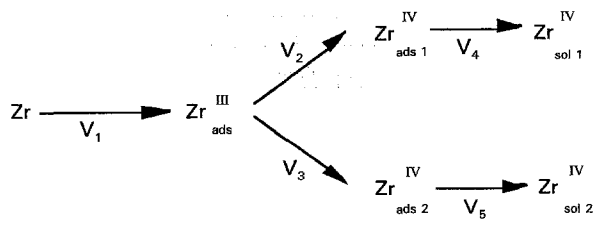

Fig. 2. Five determining step model: three electrochemical steps (rates V_1, V_2 and V_3), two chemical steps (rates V_4 and V_5).

Table 1. Alloying element and impurity contents in zirconium and Zircaloy 4

Elements	*Fe*	*Cr*	*Sn*	*Hf*	*C*	*O*	*H*	*N*
Zirconium/ppm	38	<10	<30	61	45	160	40	11
Zircaloy 4/ppm	2000	1100	12950	52	144	1350	<10	33

up to +1000 mV vs SCE, to those obtained in a previous study with less strict control of the experimental conditions [1]. These findings confirmed the existence of three distinct potential areas, each corresponding to a different behaviour: (I) activation range, (II) passivation range with low negative slope and (III) passivation range with higher negative slope.

Moreover, a fourth area (IV) occurred above +1000 mV vs SCE. It corresponded to an abrupt passivation phase followed by the beginning of a low current passivity plateau. This type of passivation was verified in several experiments. The phenomenon was reversible, and polarization towards more cathodic potentials gave rise to current values very similar to those measured when increasing potential polarization. This is one way of confirming that variations in the composition of the solution can be neglected. The last plateau was difficult to define, mainly because of the spontaneous peeling of the tetravalent zirconium oxide layer. This phenomenon is typical of the formation of ZrO_2 in various media, including nitric acid [12] and pressurized hot water [13]. The adhesion of the oxide film is particularly sensitive to hydrodynamic disturbances generated, for example, by a change in the rotation speed of the disc. This explains the difficulty in obtaining a steady-state current in this potential range and warranted the extra precautions taken in this study. The experimental points plotted in the passivity range correspond to the minimum current attainable before breakdown of the passive film. They do not, therefore, exactly represent the steady state of the electrochemical system under study. Considering behaviour

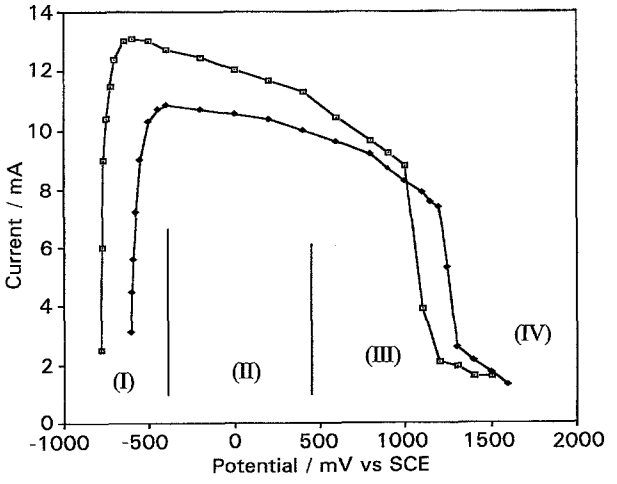

Fig. 3. Current–potential curves for zirconium (□) and Zircaloy 4 (◆) in (NaF: 0.12 M + HNO_3: 7 M); diam. 5 mm; 500 rpm; 25 °C.

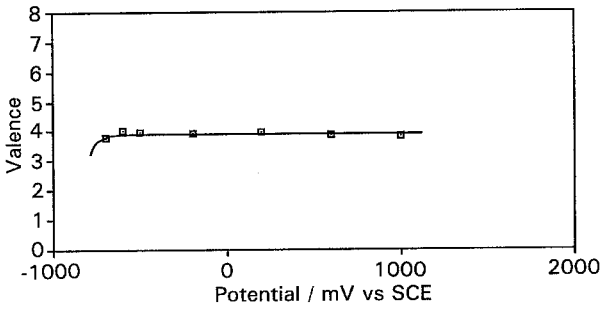

Fig. 4. Variation of the valence state of dissolved zirconium with potential.

differences between zirconium and Zircaloy 4, variations were relatively small as (I, E) profiles were maintained. The main changes were a few shifts in corrosion and passivation potentials, as well as a lower current value for Zircaloy 4.

3.2. *Valence of dissolved species*

The valence of dissolved zirconium ions was measured by the mass loss method. Its variation with potential (Fig. 4) showed a plateau at a value of 4 over the entire activity domain. Previous results obtained with Zircaloy 4 [1] were thus ascertained for zirconium.

3.3. *Surface morphology*

Characteristically corroded surfaces for domains (II) and (III) are presented for zirconium and Zircaloy 4 in Figs 5 and 6, respectively. Despite great differences (probably due to the alloying element content of zircaloy 4), the variation between the surface state with potential was similar. A degree of modification was found in both cases between domain (II) and domain (III), with a more marked contrast between the areas of different crystalline orientation (grains); this very likely corresponds with the formation of different compounds in these potential ranges and may be related to a visibly lower quality of the surface polish in domain (III) relative to domain (II). At potentials over +1000 mV vs SCE, both surfaces were covered with an insulating black zirconia film. Unfortunately, it was impossible to study the presence of the different compounds by X-ray analysis because of the natural passivation tendency of zirconium by ZrO_2 in water or air [12, 13].

4. Discussion

The shape of the curves obtained differs perceptibly from published data [8, 9, 11], probably owing to very different experimental conditions. A very

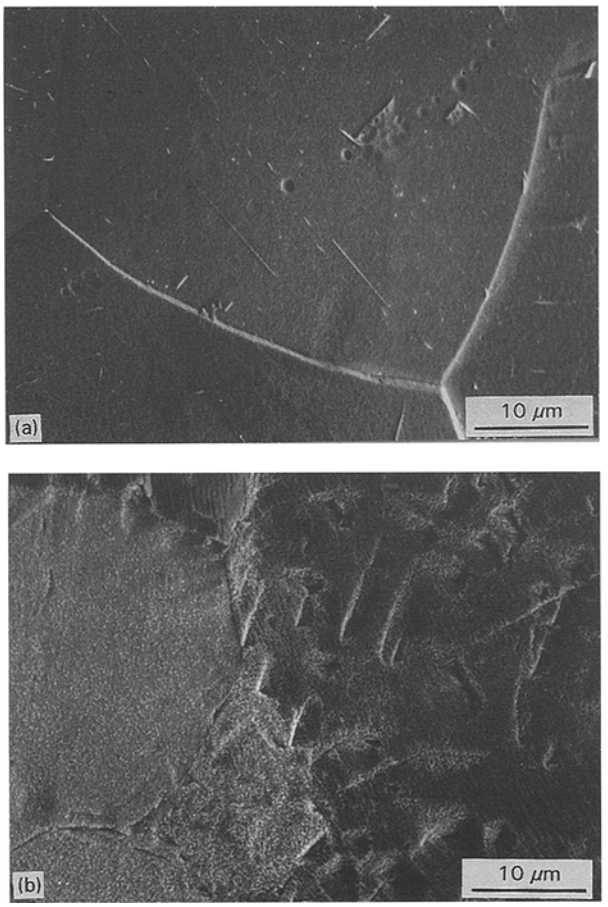

Fig. 5. SEM photograph of the surface of zirconium Van Arkel in (NaF: 0.12 M + HNO_3: 7 M). (a) −600 mV vs SCE, 1 h at 25 °C; (b) +900 mV vs SCE, 1 h at 25 °C.

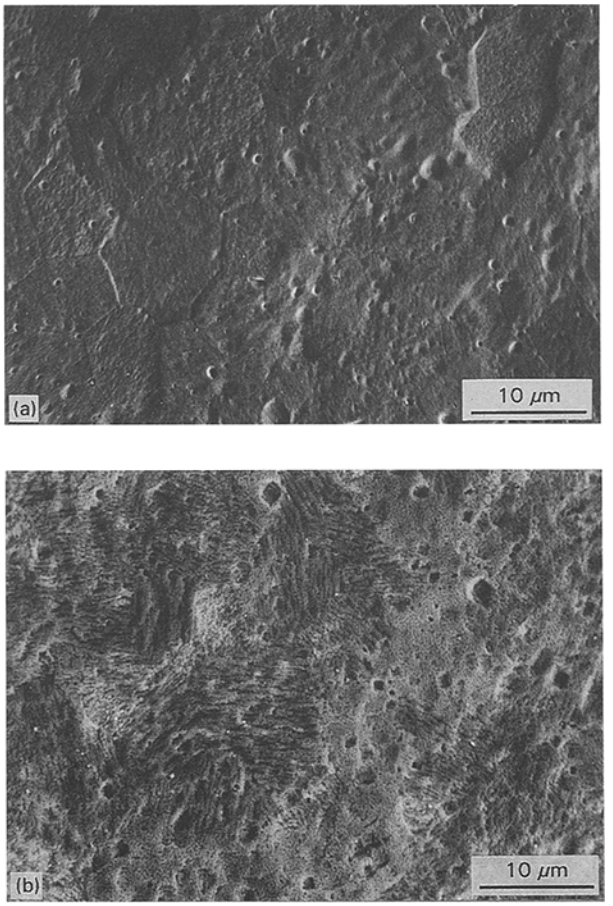

Fig. 6. SEM photograph of the surface of Zircaloy 4 in (NaF: 0.12 M + HNO_3: 7 M). (a) −400 mV vs SCE, 1 h at 25 °C; (b) +800 mV vs SCE, 1 h at 25 °C.

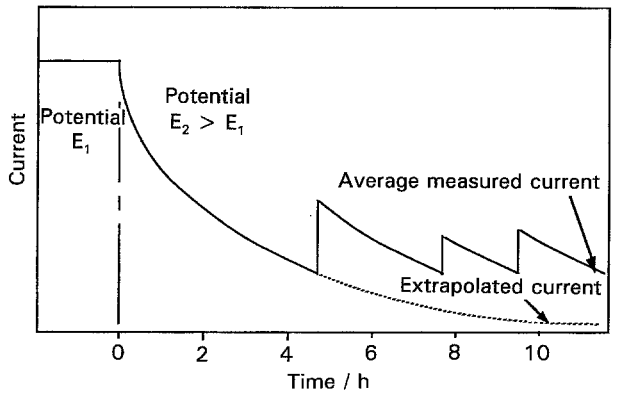

Fig. 7. Schematic variation of current against polarization time ($E_1 > 1000$ mV vs SCE); solid line: values reported on Fig. 3; dotted line: values taken into account for computation.

narrow potential range (less than 400 mV wide), which makes it impossible to examine the complete activity domain, was used in some studies [8, 11]. Other results [9] were obtained under potentiodynamic control, which may alter the current–potential profile. Moreover, the latter does not take into account the influence of the ohmic drop and fails to control hydrodynamic conditions adequately, as a rotating disc electrode is not used. Our results should be more reliable, because they were obtained under steady-state polarization over a wide range of potential and with strictly controlled experimental conditions. Moreover, quantitative analysis of current-potential curves, as described in the introduction [1–7], makes it compulsory to consider steady-state measurements only.

This new experimental approach highlighted a decisive transition towards a passive state at potentials higher than +1000 mV vs SCE. Unfortunately, difficulties are rapidly encountered in obtaining steady state, and the precise determination of a passivity current is impossible. The pseudo-plateau (domain IV) described above thus results from a particular interpretation of experimental data; this has no consequences for global analyses but makes perfect quantitative analysis impossible.

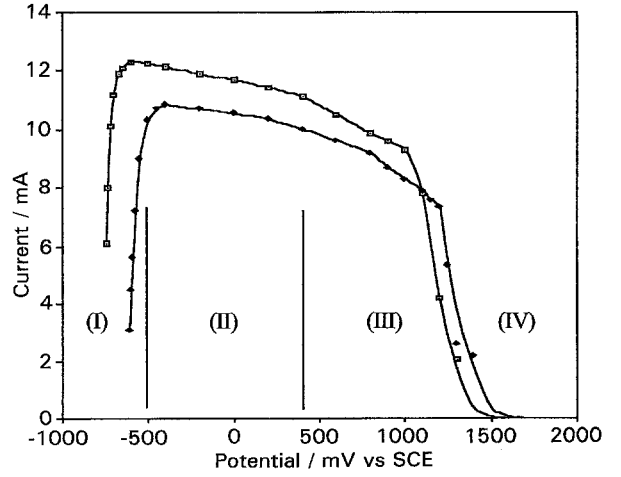

Fig. 8. Current–potential curves with corrected passive plateau for zirconium (□) and Zircaloy 4 (◆) in (NaF: 0.12 M + HNO_3: 7 M); diam. 5 mm; 500 rpm; 25 °C.

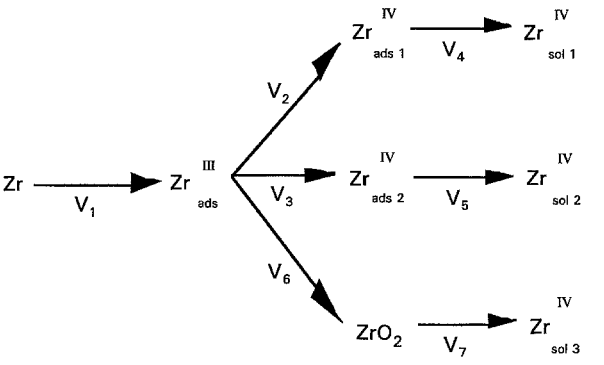

Fig. 9. Seven determining step model: four electrochemical steps (rates V_1, V_2, V_3 and V_6); two chemical steps (rates V_4, V_5 and V_7).

In this potential range, the zirconia film covering the metal is subject to the combined effects of both its formation kinetics and aggression by fluorinated species. Indeed, a characteristic peeling phenomenon is observed and the current plotted in the passive region (Fig. 3) is the one preceding a random 'increase-decrease' intensity progression corresponding to oxide 'formation-destruction'. As a result, the determination of a real passive current is difficult and takes much longer than the method used to obtain the data reported in Fig. 3. Despite these disturbances of the (current, time) graph schematically presented in Fig. 7, we can extrapolate a monotonic evolution leading, for each potential, to a very low value. These values were used for computation at potentials over +1000 mV vs SCE.

The final shape of the polarization curves for zirconium (Van Arkel) and Zircaloy 4 in the media (0.12 mol dm^{-3} NaF + 7 mol dm^{-3} HNO_3) are presented in Fig. 8. As far as modelling is concerned, it is necessary to take into account the part played by zirconia in the passivation process. The valence state of dissolved ions being unchanged over +1000 mV vs SCE, the simplest solution is to create a third branch in the five-step model (Fig. 2). In this branch, originating from Zr^{III}_{ads}, zirconia is considered as a low soluble intermediate species. The new model is presented in Fig. 9.

For both materials, surface morphology (Figs 5 and 6) examination confirms this statement. The differences in the surface state, between domain (II) (about −400 mV vs SCE) and domain (III) (about +800 mV vs SCE), are also compatible with different dissolution processes. Moreover, these morphologies differed strongly from those obtained at potentials

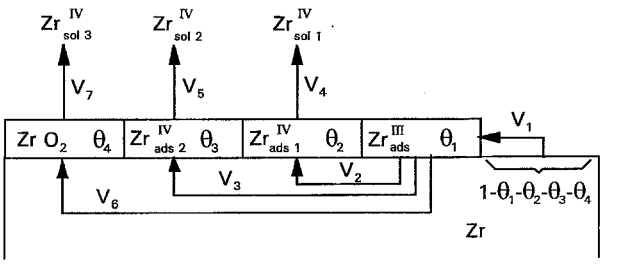

Fig. 10. Schematic presentation of the zirconium-fluonitric medium interface with zirconia consideration.

higher than +1000 mV vs SCE (not shown), at which the surfaces were totally covered with a black oxide film. This is further evidence for a reaction mechanism composed of several competing paths that can predominate in precise potential ranges.

This leads to the interface scheme shown in Fig. 10. The reaction rates related to each step can be expressed as a function of the covering ratio of intermediate species:

$$V_1 = K_1(1 - \theta_1 - \theta_2 - \theta_3 - \theta_4)$$
$$V_2 = K_2\theta_1$$
$$V_3 = K_3\theta_1$$
$$V_6 = K_6\theta_1$$
$$V_4 = K_4\theta_2$$
$$V_5 = K_5\theta_3$$
$$V_7 = K_7\theta_4$$

At steady state, the following equalities can be found:

$$V_1 = V_2 + V_3 + V_6$$
$$V_2 = V_4$$
$$V_3 = V_5$$
$$V_6 = V_7$$

The expression for the steady-state current, I, and the covering ratio, θ_1, can be inferred:

$$I = 4\mathcal{F}(K_2 + K_3 + K_6)\theta_1 \quad (1)$$

$$\theta_1 = \frac{1}{1 + K_2\left(\frac{1}{K_1} + \frac{1}{K_4}\right) + K_3\left(\frac{1}{K_1} + \frac{1}{K_5}\right) + K_6\left(\frac{1}{K_1} + \frac{1}{K_7}\right)} \quad (2)$$

Then, by introducing Equation 2 in Equation 1:

$$I = \frac{4\mathcal{F}(K_2 + K_3 + K_6)}{1 + K_2\left(\frac{1}{K_1} + \frac{1}{K_4}\right) + K_3\left(\frac{1}{K_1} + \frac{1}{K_5}\right) + K_6\left(\frac{1}{K_1} + \frac{1}{K_7}\right)} \quad (3)$$

The rates of electrochemical steps can be expressed by: $K_i = K_i^0\, e^{k_i E}$ where K_i^0 represents the rate constant and k_i the Tafel exponent

$K_1 = A\, e^{aE}$ rate of the electrochemical step:

$Zr \rightarrow Zr^{III}_{ads}$

$K_2 = B_1\, e^{b_1 E}$ rate of the electrochemical step:

$Zr^{III}_{ads} \rightarrow Zr^{IV}_{ads1}$

$K_3 = B_2\, e^{b_2 E}$ rate of the electrochemical step:

$Zr^{III}_{ads} \rightarrow Zr^{IV}_{ads2}$

$K_6 = B_3\, e^{b_3 E}$ rate of the electrochemical step:

$Zr^{III}_{ads} \rightarrow Zr^{IV}_{ads3}$

K_4, K_5, K_7 rate of chemical dissolution of the species Zr^{IV}_{ads1}, Zr^{IV}_{ads2} and Zr^{IV}_{ads3}, respectively.

Finally, the current–potential relation (3) becomes:

$$I = 4\mathcal{F}(B_1\, e^{b_1 E} + B_2\, e^{b_2 E} + B_3\, e^{b_3 E}) \div 1 + B_1\, e^{b_1 E}\left(\frac{1}{A\, e^{aE}} + \frac{1}{K_4}\right) + B_2\, e^{b_2 E}\left(\frac{1}{A\, e^{aE}} + \frac{1}{K_5}\right) + B_3\, e^{b_3 E}\left(\frac{1}{A\, e^{aE}} + \frac{1}{K_7}\right) \quad (4)$$

This relation does not show the diffusional component of the dissolution kinetics, although diffusion control is mentioned by all authors and verified here.

The aim of this work was to take into account and model the rates of emergence and disappearance of intermediate species, with a view to defining a reaction scheme. Thus, the diffusion kinetics through the electrolyte of reagents or reaction products (Zr^{IV}_{sol1} and Zr^{IV}_{sol2}; ZrO_2 is assumed to be quasiinsoluble) is integrated into the rate constants (K_4, K_5, K_7) representing their chemical dissolution. A strict analysis of the diffusional component would require the study of the current-rotation speed laws on a rotating disc. This has been done in previous work [14, 15] and will be dealt with in a forthcoming paper. In fact, Relation 4 can only be used in perfectly controlled and invariable hydrodynamic conditions. These requirements were met here, through strictly controlled use of a rotating disc electrode.

An adaptation of the optimization method [1] allows the eleven kinetic parameters to be determined. The computed curves are presented in Fig. 11 for both materials. Excellent agreement with experimental steady-state (I, E) curves was found, confirming the validity of the model. The covering ratio evolutions versus the potential (Fig. 12) also shows the major importance of the first branch of the model (I) compared with the second branch (II) in the passivation range, from the maximum current potential up to +1000 mV vs SCE. This branch leads to the maximum surface covering ratio below +800 mV vs SCE. Consequently, it plays an essential part in the dissolution kinetics by maintaining a very high current intensity which characterizes the strong instability of the adsorbed species Zr^{IV}_{ads1}.

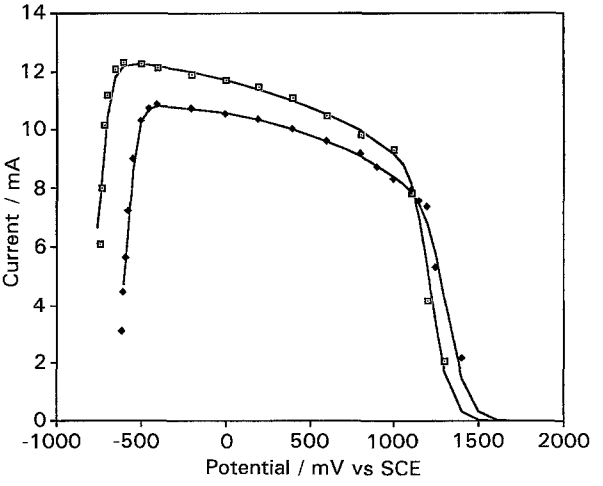

Fig. 11. Computed current-potential curve relative to the seven step model of Fig. 9 for zirconium (Van Arkel) (□) and Zircaloy 4 (◆).

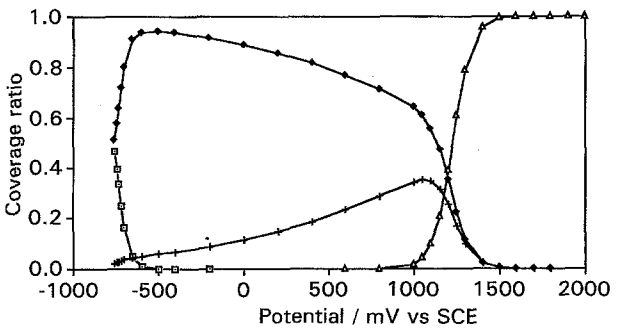

Fig. 12. Variation of the coverage ratio with potential for zirconium (Van Arkel). Key: (□) θ_1, (◆) θ_2, (+) θ_3 and (△) θ_4.

Moreover, the evolution of the covering ratios θ_2 and θ_3 can be linked to the surface state of the alloy (SEM photographs in Fig. 4). The best surface quality, observed using SEM in domain (II), was associated with the maximum occupation of the tetravalent species Zr^{IV}_{ads1}, characterized by θ_2. The reaction model, particularly through the covering ratios, can thus be useful when testing the consequences on the surface state of the parameters acting in the dissolution process.

The computed values of the kinetic parameters are given in Table 2. Tafel exponents a, b_1 and b_2 correspond to transfer coefficient values between 0 and 1, which is physically meaningful. On the other hand, in domain (IV), which corresponds to passivity, the value of b_3 is greater than 1. This may be due to the uncertainty of the experimental measurements in this domain and in no way calls into doubt the whole model. The values of the constant rates (B_2, B_3, K_5 and K_7) for branches (I) and (II) are somewhat modified relative to the previous five-step model. The modifications particularly affect B_2 and K_5. They logically follow the changes of the model and the (I,E) curves. Previously, B_2 and K_5 determined passivation and pseudo-passivity. This function is now attributed to B_3 and K_7. Moreover, B_2 and K_5 are affected by slight modifications of the (I,E) profile resulting from the second procedure below +1000 mV vs SCE.

These results illustrate the very gradual change in the passive dissolution of zirconium (pure or alloyed) versus the potential. This passivation becomes more abrupt only after +1000 mV vs SCE, in keeping with the drastic drop in current up to +1500 mV vs SCE, which is linked to the increase in the zirconia covering ratio.

Table 2. Kinetic parameter values corresponding to the computed (I,E) curves of Fig. 11

Parameters	*Zirconium*	*Zircaloy 4*
a/mV^{-1}	0.021	0.017
b_1/mV^{-1}	0.023	0.026
b_2/mV^{-1}	0.024	0.028
b_3/mV^{-1}	0.045	0.047
A/mmol cm^{-2} s^{-1}	4.8×10^{18}	0.92×10^{19}
B_1/mmol cm^{-2} s^{-1}	3.5×10^{3}	1.3×10^{3}
B_2/mmol cm^{-2} s^{-1}	1.4×10^{2}	3.2×10^{1}
B_3/mmol cm^{-2} s^{-1}	7.6×10^{-13}	4.2×10^{-13}
K_4/mmol cm^{-2} s^{-1}	1.6×10^{-4}	1.45×10^{-4}
K_5/mmol cm^{-2} s^{-1}	5.3×10^{-5}	4.3×10^{-5}
K_7/mmol cm^{-2} s^{-1}	1.3×10^{-8}	1.3×10^{-8}

5. Conclusion

Despite their complexity and dependence on mass transport, the steady-state current–potential profiles obtained using a rigorous experimental procedure have been interpreted using a reaction model validated by computer-experimental comparison. This model is characterized by three reaction paths, each governing in turn the dissolution kinetics of zirconium in fluorinated nitric media. Depending on the potential range, these three branches lead to the dissolution of three tetravalent zirconium compounds, zirconia being the most passivating species. This model, and the conclusions drawn from it, differs from the approaches used by previous authors. When the study was restricted to potentials from E_{corr} to −400 mV vs SCE, the current–potential curve could be considered a pure diffusion plateau. In our model, this situation amounts to neglecting the influence of the second and third branches in this potential range. However, accurate analysis of a wide potential domain shows that this hypothesis is a simplification which does not take into account the very gradual modification of the surface coverage towards more passive species.

Previous authors considered that ZrO_2 oxide was the only species formed at the interface and that it was involved, as an intermediary, in the dissolution of zirconium. Our study shows that the oxide only emerges at very anodic potentials, corresponding to a surface passivation over +1000 mV vs SCE.

This confusion results from the limited methods available for physically identifying the products of electrochemical reactions. Thus, the short-lived intermediates present on the surface during dissolution are probably replaced by an oxide layer during rinsing or exposure to the atmosphere. As *in situ* surface analysis during dissolution is very difficult, electrochemistry appears to be the most suitable method for proving the existence of short-lived intermediates.

Concerning the relation between the reaction scheme and surface quality, it has also been shown that the first branch, which is most strongly influenced by diffusional mass transport [14], is also the best-adapted to the pickling process. This branch is predominant at potentials ranging from the maximum current potential up to about +500 mV vs SCE. This range is reduced in the case of Zircaloy 4.

Consequently, this model should prove an interesting tool for evaluating the influence of various factors on the zirconium dissolution process in fluorinated nitric media. A first examination can be carried out on the alloying elements of a low alloyed zirconium (5 to 6%) compared with the dissolution of pure metal. A further study will be conducted using binary alloys to determine the influence of tin and niobium.

Acknowledgements

We thank ZIRCOTUBE for their technical and financial support and their permission to publish these results.

References

[1] J. Prono, A. Caprani, T. Jaszay and J. P. Frayret, Proceedings of the 5th International Symposium on 'Environmental Degradation of Materials in Nuclear Power Systems – Water Reactors', ANS, TMS, NACE, Monterey USA (1991) p. 175.
[2] H. Gerischer and W. Mehl, *Z. Electrochem.* **59** (1955) 1049.
[3] R. Parsons, *J. Electroanal. Chem.* **21** (1969) 35.
[4] P. Rabu, G. Saindrenan, A. Caprani, T. Jaszay and J. P. Frayret, *J. Appl. Electrochem.* **22** (1992) 57.
[5] T. Jaszay, Thèse, Nantes (1991).
[6] F. Priem, T. Jaszay, A. Caprani, S. K. Marya and J. P. Frayret, Sixth World Conference on Titanium, Cannes (1988).
[7] J. P. Badiali, H. Cachet, A. Cyrot and J. C. Lestrade, *J. Chem. Soc. Faraday Trans. II* **69** (1973) 1339.
[8] R. E. Meyer, *J. Electrochem. Soc.* **111** (1964) 147.
[9] E. M. M. Sutter, F. Hlawka and A. Cornet, *Corrosion* **46** (1990) 537.
[10] V. G. Levitch, 'Physicochemical Hydrodynamics', Prentice Hall, NJ (1962).
[11] R. E. Meyer, *J. Electrochem. Soc.* **112** (1965) 684.
[12] R. D. Misch and W. E. Ruther, *J. Electrochem. Soc.* **100** (1953) 531.
[13] K. Ogata, 'Zirconium in the Nuclear Industry', ASTM, (1989) pp. 346–359.
[14] J. Prono, F. Priem, T. Jaszay, A. Caprani and J. P. Frayret, 41st Meeting of ISE, Prague, Czechoslovakia, 20–25 Aug (1990) Fr-155
[15] J. Prono, Thèse, Nantes (1993).